ISPRS Journal of Photogrammetry and Remote Sensing 104 (2015) 213–223

Contents lists available at ScienceDirect

ISPRS Journal of Photogrammetry and Remote Sensing

journal homepage: www.elsevier.com/locate/isprsjprs

Applying data fusion techniques for benthic habitat mapping and monitoring in a coral reef ecosystem

Caiyun Zhang *

Department of Geosciences, Florida Atlantic University, Boca Raton, FL 33431, United States

ARTICLE INFO

Article history:
Available online 27 June 2014

Keywords:
Data fusion
Machine learning
Benthic habitat mapping
Hyperspectral imagery
Object-based image analysis
Coral reef ecosystem

ABSTRACT

Accurate mapping and effective monitoring of benthic habitat in the Florida Keys are critical in developing management strategies for this valuable coral reef ecosystem. For this study, a framework was designed for automated benthic habitat mapping by combining multiple data sources (hyperspectral, aerial photography, and bathymetry data) and four contemporary imagery processing techniques (data fusion, Object-based Image Analysis (OBIA), machine learning, and ensemble analysis). In the framework, 1-m digital aerial photograph was first merged with 17-m hyperspectral imagery and 10-m bathymetry data using a pixel/feature-level fusion strategy. The fused dataset was then preclassified by three machine learning algorithms (Random Forest, Support Vector Machines, and *k*-Nearest Neighbor). Final object-based habitat maps were produced through ensemble analysis of outcomes from three classifiers. The framework was tested for classifying a group-level (3-class) and code-level (9-class) habitats in a portion of the Florida Keys. Informative and accurate habitat maps were achieved with an overall accuracy of 88.5% and 83.5% for the group-level and code-level classifications, respectively.

1. Introduction

1.1. Importance of Florida Keys and benthic habitat mapping

The Florida Keys, a delicate chain of islands extending from the southern tip of Florida, are the third largest barrier reef ecosystem in the world. The keys and their marine environment support a series of natural habitats including coral reefs, seagrass, and mangroves, which attract many recreational, commercial, and scientific activities. The ecosystem in the Florida Keys has long been threatened by global climate change (e.g., ocean warming), human activities (e.g., fishing and pollution), hurricanes, and tropical storms (Rohmann and Monaco, 2005). The preservation of the Florida Keys ecosystem has become a national priority (Rohmann and Monaco, 2005).

Benthic habitats are places on or near the sea floor where aquatic organisms live. These beds of seagrass, coral reef, areas of mud, and sand provide shelters to a rich array of animals. It is widely recognized the need to map benthic habitats for the reef environment in order to provide rapid assessment of health and stress response of these vulnerable ecosystems. A range of research projects has been conducted in the conservation and management of the Florida Keys (Florida Keys National Marine Sanctuary, <http://floridakeys.noaa.gov/>), many of which need the benthic habitat information of this area. Precise mapping of benthic habitats in the Florida Keys is critical for developing management strategies that balance the protection of these habitats with their use (Rohmann and Monaco, 2005).

1.2. Application of hyperspectral systems in benthic habitat mapping

Major mapping efforts of benthos in the Florida Keys have focused on the visual interpretation of fine scale aerial imagery with assistance from other data sources such as bathymetry data (Rohmann and Monaco, 2005). With the emergence of hyperspectral systems, it has been anticipated that this procedure can be superseded by automated digital image analysis. Hyperspectral sensors collect data in hundreds of relatively narrow spectral bands throughout the visible and infrared portions of the electromagnetic spectrum. They are more powerful than traditional multispectral sensors in habitat discrimination due to their rich radiometric contents. The application of hyperspectral systems has become an important area of research in characterizing benthos in the past decade (e.g., Mishra et al., 2007; Lesser and Mobley, 2007; Phinn et al., 2008; Bertels et al., 2008; Fearns

* Tel.: +1 561 297 2648.
E-mail address: czhang3@fau.edu

http://dx.doi.org/10.1016/j.isprsjprs.2014.06.005
0924-2716/

et al., 2011; Pu et al., 2012; Botha et al., 2013; Zhang et al., 2013). However, most of the available hyperspectral sensors such as EO-1/Hyperion and Airborne Visible/InfraRed Imaging Spectrometer (AVIRIS) collect data with a relatively coarse spatial resolution (i.e. 4 m or larger). This may limit their broad applications over regions where the distribution of benthos is highly heterogeneous or communities are present in the form of small patches or linear/narrow shapes (Zhang et al., 2013). Such limitations may be overcome by data fusion techniques, which integrate data and information from multiple data sources to achieve refined/improved information. With the increasing availability of multi-sensor and multi-resolution images, data fusion has become a valuable tool in image interpretation (Solberg, 2006; Zhang, 2010). Many researchers have combined hyperspectral imagery with Light Detection and Ranging (LiDAR) or Synthetic Aperture Radar (SAR) data to improve land characterization (Zhang and Xie, 2013a). However a synergy of hyperspectral data with fine spatial resolution optical imagery has not been well explored for the same purpose. Fusion of hyperspectral imagery, fine spatial resolution aerial photography, and bathymetry data for mapping and monitoring habitats in an aquatic environment is even scarcer.

1.3. Classification algorithms in benthic habitat mapping

Image classification is a crucial stage in remote sensing image analysis and the selection of classifiers may largely impact the final result (Benfield et al., 2007). Previous benthic habitat mapping studies most commonly applied the traditional image classifiers such as Maximum Likelihood (ML) (e.g., Mumby and Edwards, 2002; Andréfouët et al., 2003; Benfield et al., 2007; Pu et al., 2012; Zapata-Ramírez et al., 2013). ML method requires the spectral response of each class to follow a Gaussian distribution, which is not guaranteed for hyperspectral data. Contemporary machine learning techniques have received little attention in benthic habitat mapping, although they can produce higher accuracies than ML classifier, especially in classifying hyperspectral data (Zhang and Xie, 2012; 2013a,b). There is a need to expand machine leaning techniques into benthic habitat mapping as an alternative to ML algorithm.

Previous studies have shown that three machine learning algorithms Random Forest (RF), Support Vector Machines (SVMs), and *k*-Nearest Neighbor (*k*-NN) are promising in classifying hyperspectral imagery (e.g., Ham et al., 2005; Chan and Paelinckx, 2008; Waske et al., 2009; Mountrakis et al., 2010; Zhang and Xie, 2013a,b; Zhang et al. 2013). For this study, the performance of RF, SVMs, and *k*-NN was evaluated to classify a fused dataset from hyperspectral imagery, aerial photography, and bathymetry data. The classification results from RF, SVMs, and *k*-NN may be different for each class. A combination of the strengths of each classifier may have the potential to achieve a better mapping result through ensemble analysis techniques. Thus, classifier ensemble techniques were also evaluated.

1.4. Mapping methods

Most researchers mapped the benthos at the pixel level, which may lead to the "salt-and pepper" effect if the mapping area has diverse habitats with high spatial heterogeneity. It has been well documented that this issue can be overcome by Object-Based Image Analysis (OBIA) techniques which first decompose an image scene into relatively homogeneous areas and then classify these areas instead of pixels. OBIA has been well developed and applied in terrestrial studies, as evidenced by a review paper from Blaschke (2010). However, such methods have not been utilized sufficiently in benthic habitat mapping. Benfield et al. (2007) compared the object- and pixel-based methods in mapping coral reefs and associated sublittoral habitats using multispectral imagery. They found that object-based classifications can produce more accurate results than pixel-based approaches. Phinn et al. (2012) applied the OBIA techniques for mapping geomorphic and ecological zones of coral reefs. They found that OBIA is effective to explicitly map regional scale benthic community composition from fine spatial resolution satellite imagery. To produce informative (i.e. without salt-and-pepper effect) habitat maps, the object-based mapping methods are desirable.

1.5. Objectives of this study

Data fusion, OBIA, machine learning algorithms, and ensemble analysis have been extensively applied in terrestrial remote sensing studies (Waske et al., 2009; Zhang, 2010; Blaschke, 2010; Du et al., 2012), but a combination of these techniques for habitat characterization in aquatic environments are limited. For this study, a framework was designed to combine these techniques for object-based benthic habitat mapping in the Florida Keys. In this framework, a pixel/feature-level fusion strategy was developed to merge 1-m aerial photograph, 17-m AVIRIS imagery, and 10-m bathymetry data. Three popular machine learning classifiers RF, SVMs, and *k*-NN were examined to pre-classify the fused dataset. Final classified habitat maps were produced through ensemble analysis of outcomes from three machine learning classifiers. The main objective of this study is to explore whether data fusion techniques can improve benthic habitat classification accuracy in a coral reef ecosystem the Florida Keys.

2. Study site and data

2.1. Study site

The study area, with an approximate size of 40 km^2, is located in the lower Florida Keys (Fig. 1). The Florida Keys are a coral cay archipelago beginning at the southeastern tip of the Florida peninsula and extending in a gentle arc south-southwest and then westward to the inhabited islands known as Key West. The study site has a tropical climate and its environment is similar to the Caribbean. This area is characterized by spectacular coral reefs, extensive seagrass beds, and mangrove-fringed islands. It is one of the world's most productive ecosystems with more than 6000 species of marine life and 250 species of birds nesting in this region. The water depth in the study area varies from 0 meter to 6.4 m. The substrate consists of hardbottom, continuous seagrass, and patch seagrass for the selected region.

2.2. Data

Data sources used in this study include AVIRIS hyperspectral imagery, aerial photography, bathymetry data, and benthic habitat reference maps. AVIRIS collects calibrated hyperspectral data in 224 contiguous spectral channels with wavelengths from 0.4 μm to 2.5 μm. AVIRIS data over the study area were collected on November 19, 1992 with a spatial resolution of 17 m. Fine spatial resolution aerial photographs were collected on January 15, 1994 by the National Aerial Photography Program (NAPP). The U. S. Geological Survey (USGS) orthorectified these aerial photographs into data products known as Digital Orthophoto Quarter Quads (DOQQs). The accuracy and quality of DOQQs meet National Map Accuracy Standards. DOQQs with a spatial resolution of 1 meter were used for this study. DOQQs also provide a base to georeference the hyperspectral data. The bathymetry data are from the National Geophysical Data Center (NGDC) of National Oceanic and Atmospheric Administration (NOAA). The NGDC

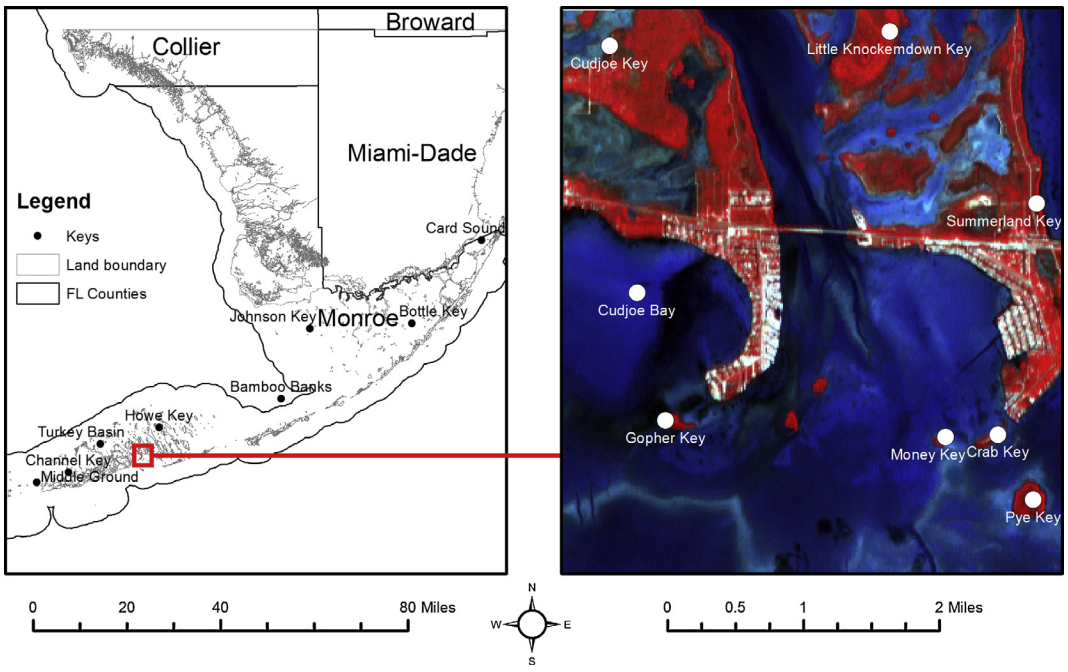

Fig. 1. Maps of the Florida Keys and study area shown in a color composite generated from AVIRIS data.

produced a Digital Elevation Model (DEM) with a spatial resolution of 1/3 arc-second (~10 m) for the Florida Keys by combining many available elevation data sources (Grothe et al., 2011). The benthic habitat reference data were produced through a seven-year project cooperatively conducted by the National Ocean zService of NOAA and the Florida Fish and Wildlife Research Institute. In this project benthic habitats were visually interpreted using stereo analytical plotters from a series of aerial photographs collected between December 1991 and April 1992. Final benthic habitat maps were produced and calibrated through extensive field data. This dataset was released to the public in 1998 (Benthic Habitats of the Florida Keys, <http://flkeysbenthicm-aps.noaa.gov/>). Habitats were classified into 4 major categories (referred to as the group-level classes) and 24 subcategories (referred to as the code-level classes) based on a classification scheme developed in the project. This dataset is currently serving as the baseline in the management of Florida Keys. Updating these maps is difficult because manual interpretation procedure is time consuming and labor intensive.

Fig. 3a (top two panels) shows the group- and code-level reference maps for the study site. Three group-level communities were found: hardbottom, continuous seagrass, and patchy seagrass. Six code-level habitats were observed: HC (*soft coral, hard coral, sponge, and algae hardbottom*), HS (*hardbottom with perceptible seagrass (<50%)*), SD (*moderate to dense, continuous beds of seagrass*), SDB (*moderate to dense nearly continuous beds (seagrass > 50%), with blowouts and/or sand or mud patches*), SPH (*dense patches of seagrass (>50%) in a matrix of hardbottom*), and SS (*sparse continuous beds of seagrass*). The code-level habitats located over the banks have distinctive signatures on the aerial photographs, thus they were separately denoted in the reference map, resulting in three extra codes: HSb, SDb, and SDBb. Descriptions of these habitats in the project are listed in the Appendix Table. A total of 786 sample objects were spatially randomly selected by following a stratified random sampling strategy in which a fixed percentage of samples are selected for each class. The number of samples for each class was roughly estimated based on the image segmentation result and reference maps. The image segmentation procedure is detailed in the Methodology section. The selected sample data were split into two halves with one used for calibration (training) and the other used for validation (testing).

3. Methodology

3.1. Data preprocessing

Spectral channels with a low signal-to-noise ratio and strong water absorption were dropped from the AVIRIS imagery, leading to 30 visible bands for further analysis. An image to image rectification was employed to georeference AVIRIS data with the use of the aerial photograph. Non-water areas were masked out using the bathymetry data. Hyperspectral data contains a tremendous amount of redundant spectral information. The Minimum Noise Fraction (MNF) method (Green et al., 1988) is commonly used to reduce the high dimensionality and inherent noise of hyperspectral data. It applies two cascaded principal component analyses, with the first transformation decorrelating and rescaling noise in the data, and the second transformation creating coherent eigenimages that contain useful information and generating noise-dominated eigenimages. The transformation generates the eigenvalues and corresponding eigenimages, both of which are used to determine the true dimensionality of the data. The MNF transformation was conducted in ENVI 4.7 and the most useful and spatially coherent eigenimages were selected. Recent study from Zhang et al. (2013) shows that the MNF transformed data of hyperspectral imagery can significantly increase accuracy of benthic habitat classification. Thus only the MNF imagery was considered in further analysis. In benthic habitat mapping, researchers most commonly conducted three image preprocessing procedures (atmospheric, sun-glint, and water-column corrections) to predict the reflectance from the water bottom. Zhang et al. (2013) systematically evaluated the impact of three corrections on benthic habitat classification in the Florida Keys. They found that these three preprocessing procedures are unnecessary for benthic habitat

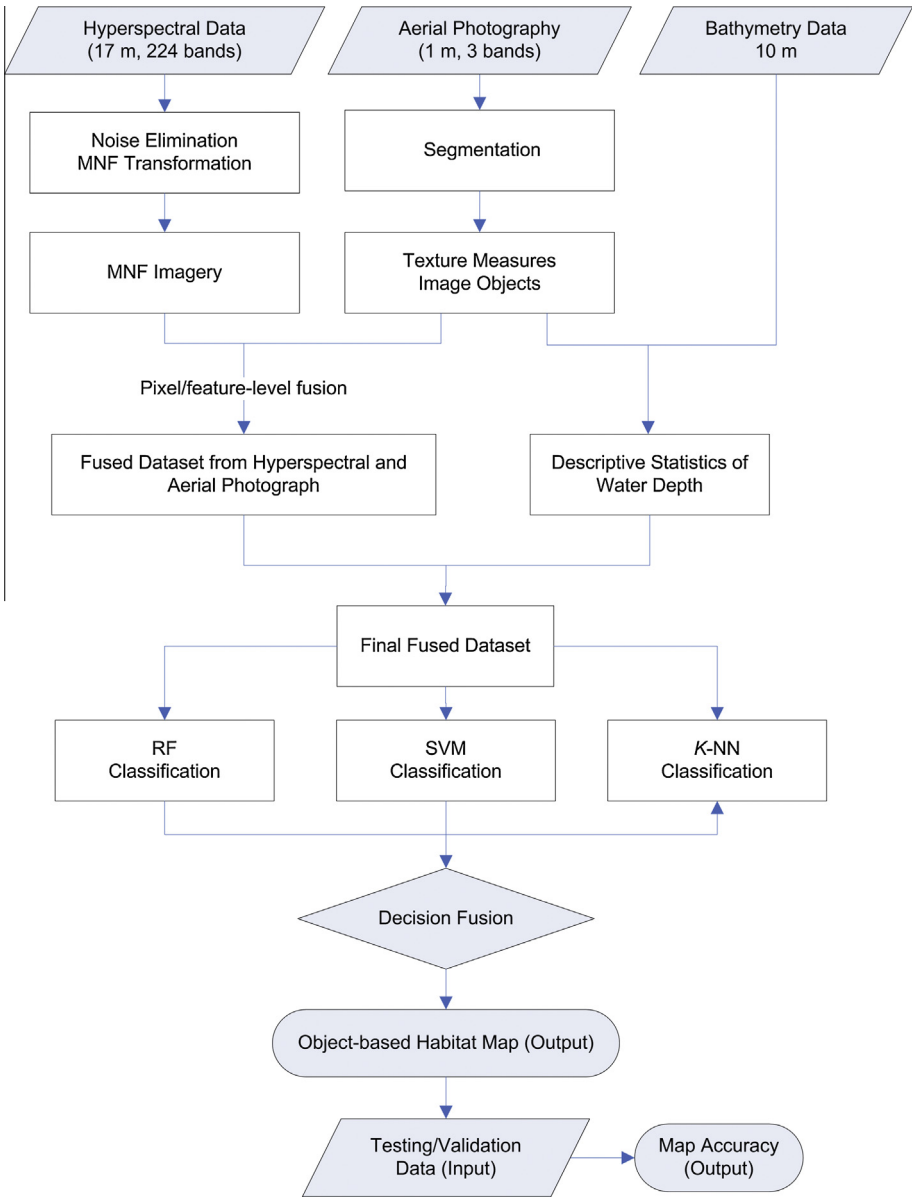

Fig. 2. The designed framework to combine hyperspectral imagery, aerial photography, and bathymetry data for benthic habitat mapping.

mapping in the Florida Keys. Thus for this study, three corrections were not carried out.

3.2. A framework to fuse hyperspectral imagery, aerial photograph, and bathymetry data

Data fusion methods can be grouped into three categories: pixel-level fusion, feature-level fusion, and decision-level fusion (Zhang, 2010). Pixel-level fusion combines raw data from multiple sources into single resolution data to improve the performance of image processing tasks. Information may be lost during the data resampling procedure if the spatial resolution of input data sources is different (Solberg, 2006). Feature-level fusion extracts features (e.g., edges, corners, lines, and textures) from each individual data source and merges these features into one or more feature maps for further processing. Combination of these features consists of complex procedures. Decision-level fusion commonly conducts a preliminary classification for each individual data source first, and then combines the classification results into one outcome based on a decision fusion strategy.

For this study a framework is designed to combine all three data fusion methods to fuse three data sources, as shown in Fig. 2. In the framework, 1-m aerial photograph is segmented first to generate image objects and extract object features (i.e. textures). The extracted features are then combined with pixel-level values of hyperspectral data to generate a fused dataset. This is achieved by calculating a mean spectrum of hyperspectral pixels which are geographically within an image object. The mean spectrum is then integrated with the extracted aerial textures of this image object. For the bathymetry data, descriptive statistics (minimum, maximum, mean, and standard deviation) of water depth are calculated for each image object. All the derived bathymetric features are then combined with textures of aerial photograph and mean spectrum of hyperspectral imagery, leading to a final fused dataset from three data sources. The entire fusion procedure is conducted at the object level. Since the final fused dataset is from features of aerial photography (i.e. textures), bathymetry data (i.e. descriptive

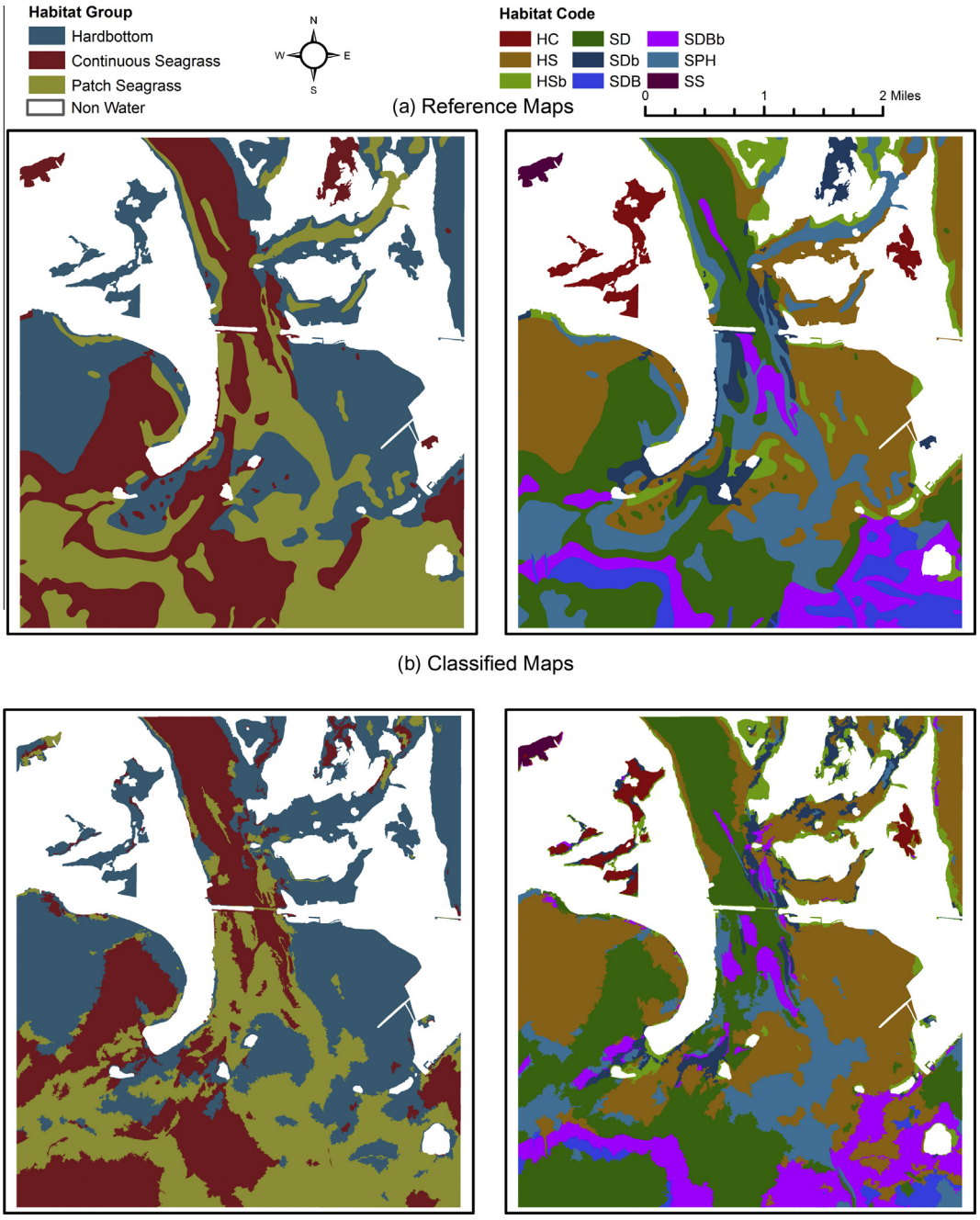

Fig. 3. Habitat maps from (a) reference data and (b) classification results of the fused dataset (hyperspectral imagery, aerial photography, and bathymetry data) and ensemble analysis of RF, SVM and *k*-NN.

statistics), and pixels of hyperspectral imagery, the fusion strategy is referred to as a pixel/feature-level fusion scheme. Four advantages are expected from this scheme: (1) no information is lost to combine three data sources because there is no data resampling in the procedure; (2) additional object-based texture information can be extracted from the aerial photography, which is useful in habitat classification; (3) small patches and linear/narrow shape habitats may be delineated due to the fine spatial resolution of aerial photography; and (4) classification uncertainties caused by the errors in the georeference procedure can be reduced. Uncertainties and errors in the georeference procedure are unavoidable, which may impact the classification results if the pixel-level data fusion scheme is adopted and classification is carried out pixel by pixel. When the object-based fusion scheme is used here, misaligned hyperspectral pixels occur at the boundary of each object. This can help reduce the classification errors because the information from the entire object is used in the classification, rather than any individual pixel. Three machine learning algorithms (RF, SVM, and *k*-NN) are used to pre-classify the final fused dataset. The ultimate outcome is derived through ensemble analysis of three classification results using a decision-level fusion strategy. Note that the decision-level fusion strategy is based on classification results of the fused dataset, rather than making a decision from classification results of the individual data sources. Consequently, an object-based habitat map is generated and evaluated based on conventional accuracy assessment approaches.

3.3. Image segmentation

Image segmentation is an important step in the framework. The multiresolution segmentation algorithm in eCognition Developer 8.64.1 (Trimble, 2011) was used to generate image objects from the aerial photograph. The segmentation algorithm starts with one-pixel image segments, and merges neighboring segments together until a heterogeneity threshold is reached (Benz et al., 2004). The heterogeneity threshold is determined by a user-defined scale parameter, as well as color/shape and smoothness/compactness weights. The image segmentation is scale-dependent, and the quality of segmentation and overall classification are largely dependent on the scale of the segmentation. In order to find an optimal scale for image segmentation, an unsupervised image segmentation evaluation approach (Johnson and Xie, 2011) was used. It begins with a series of segmentations using different scale parameters, and then identifies the optimal scale using an unsupervised evaluation method that takes into account global intra-segment and inter-segment heterogeneity measures. A global score combining a normalized weighted variance and Moran's I value is used to determine the optimal scale for the segmentation. A series of segmentations were thus carried out with the scale parameter ranging from 2 to 20, at an interval of 2. A scale parameter of 12 was found to be optimal for the study site. The weights of the MNF layers were set based on their eigenvalues. Color and shape weights were set to 0.9 and 1.0 so that spectral information would be considered more heavily for segmentation. Smoothness and compactness weights were set to 0.5 and 0.5 so as to not favor either compact or non-compact segments.

Following segmentation, object-based texture features were extracted. Object-based texture measures from fine spatial resolution imagery have been proved valuable for habitat classification (Andréfouët et al., 2003). Conventional kernel-based texture methods often utilize a fixed-size moving window over which to calculate texture measures for each pixel. It is challenging to determine the appropriate window size. OBIA offers the capability for identifying relatively homogeneous regions of varying shapes and sizes in an image. Texture extraction from image objects is more reasonable (Warner, 2011). Such object-based texture measures were thus used in this study. Both first-order and second-order metrics for each band of the aerial photography were extracted including mean, standard deviation, contrast, dissimilarity, homogeneity, entropy, and angular second moment. The Grey Level Co-occurrence Matrix (GLCM) algorithm was used to extract the second-order texture measures. The directionally invariant texture measures were produced by calculating the mean of the texture results in all four directions (0°, 45°, 90°, and 135°). Detailed calculations of these texture measures can be found in Trimble (2011).

3.4. Classification algorithms: RF, SVM, and k-NN

RF, SVM, and *k*-NN algorithms were employed to pre-classify the fused dataset. RF is a decision tree based ensemble classifier. To understand this algorithm, it is helpful to first know the decision tree approach. The decision tree splits training samples into smaller subdivisions at "nodes" using decision rules. For each node, tests are performed on the training data to find the most useful variables and variable values for split. The RF consists of a combination of decision trees where each decision tree contributes a single vote for assigning the most frequent class to an input vector. RF increases the diversity of decision trees to make them grow by changing the training set using the bagging aggregating (Breiman, 2001). Bagging creates training data by randomly resampling the original dataset with replacement. Data selected from the input sample for generating the next subset is not deleted. Different algorithms can be used to generate the decision trees. The RF often adopts the Gini Index (Breiman, 2001) to measure the best split selection. More descriptions of RF can be found in Breiman (2001) and in remote sensing context in Chan and Paelinckx (2008). Two parameters need to be defined in RF: the number of decision trees to create (k) and the number of randomly selected variables (m) considered for splitting each node in a tree.

SVM is a non-parametric supervised learning classifier. The aim of SVMs is to find a hyperplane that can separate the input dataset into a discrete predefined number of classes in a fashion consistent with the training samples (Vapnik, 1995). Research of SVMs in remote sensing has increased in the past decade, as evidenced by a review in Mountrakis et al. (2010). Detailed descriptions of SVMs were given by Huang et al. (2002) in the context of remote sensing. Kernel based SVMs are commonly used for remote sensing image classification, among which the radial basis function (RBF) and the polynomial kernels are frequently employed. RBF needs to set the kernel width (γ), and polynomial kernel needs to set the degree (p). Both kernels need to define a penalty parameter (C) that controls the degree of acceptable misclassification. The setting of these parameters can be determined by a grid search strategy which tests possible combinations of them in a user-defined range (Hsu et al., 2010). The SVM classifier was implemented using a SVM library (LIBSVM) developed by Chang and Lin (2011). Both kernels were tested to find the best model for the fused dataset.

k-NN is another supervised classifier which identifies objects based on the closest training samples in the feature space. It searches away from the unknown object to be classified in all direction until it encounters k user-specified training objects. It then assigns the object to the class with the majority vote of the encountered objects. The algorithm requires all the training data participate in each classification, thus has a slow speed of execution for pixel-based classification (Hardin, 1994). However, for the object-based classification used in this study image objects are minimum classification units, i.e., classification primitives, instead of individual pixels. The amount of classification primitives is greatly reduced through the segmentation process. Therefore computation complexity is not a problem for implementing this algorithm.

3.5. Ensemble analysis

The final classification was conducted through an ensemble analysis of the outputs from RF, SVM, and *k*-NN. An ensemble analysis approach is a multiple classification system with the aim to obtain better classification by combining the outputs of several classifiers. The classifiers in the system generally should produce accurate results but show some differences in classification accuracy (Du et al., 2012). A range of strategies have been developed to combine the outputs from multiple classifiers, such as the majority vote, Bayesian average method, and fuzzy integral approach. Among these strategies, the majority vote (each individual classifier votes for an unknown input object) is straightforward. The final class label for an input object is determined by the majority votes of classifiers. A key problem of the majority vote is that all the classifiers have equal rights to vote without considering their performances on each individual class. A weighting strategy may mitigate this problem by weighting the decision from each classifier based on their accuracies obtained from the reference data (Moreno-Seco et al., 2006). In the framework, the majority vote and the weighting strategy is combined to fuse the outputs from three classifiers. If three votes are different, then the unknown object will be assigned to the class which has the highest accuracy among the classifiers. If two or three classifiers vote the same class for an input object, then the object will be assigned to the same voted class.

3.6. Accuracy assessment

The error matrix and Kappa statistic (Congalton and Green, 2009) has served as the standard approaches in accuracy assessment. I constructed the error matrix and calculated the Kappa statistics for the classifications. The error matrix can be summarized as an overall accuracy and Kappa value. The overall accuracy is defined as the ratio of the number of validation samples that are classified correctly to the total number of validation samples irrespective of the class. The Kappa value describes the proportion of correctly classified validation samples after random agreement is removed. To evaluate the statistical significance of differences in accuracy between different classifications, the nonparametric McNemar test (Foody, 2004) was adopted. The difference in accuracy of a pair of classifications is viewed as being statistically significant at a confidence of 95% if z-score is larger than 1.96.

4. Results

4.1. Results from experimental analysis

To examine whether data fusion can increase habitat classification accuracy, three experiments were designed. Experiment 1 used the features derived from aerial photography alone; Experiment 2 used the fused dataset from hyperspectral imagery and aerial photography; and Experiment 3 used the final fused dataset from hyperspectral imagery, aerial photography, and bathymetry data. Random Forest (RF) classifier was employed in the experiments. The number of randomly selected variables for splitting node (m) was set to 3 after several trials. A number of tests using different number of trees (50–300 at an interval of 50) revealed that $k = 150$ resulted in the highest accuracy. The final classification accuracies from these three experiments are listed in Table 1. To examine the statistical significance, the Kappa z-score statistical tests were conducted based on the error matrix. The z-score values are also displayed in Table 1.

For the group-level classification, an overall accuracy of 63.6% with a Kappa value of 0.42 was obtained using aerial photography alone (Experiment 1). Fusion of hyperspectral imagery and aerial photography increased the accuracy to 86.3% with a Kappa value of 0.78 (Experiment 2). The highest accuracy was achieved by integrating hyperspectral data, aerial photograph, and bathymetry data (Experiment 3). An overall accuracy of 88.5% with a Kappa value of 0.82 was yielded. Kappa statistical tests illustrate that all the experiments produced significantly better results than a random classification. McNemar tests demonstrate that inclusion of hyperspectral imagery in the framework significantly improved the classification accuracy, but the contribution of bathymetry data was marginal. For the code-level classification, similar results were generated. Fusing hyperspectral imagery and aerial photograph increased the accuracy from 57.0% to 79.9%. Inclusion of bathymetry data further improved the accuracy to 83.5% with a Kappa value of 0.79. Kappa statistical tests show that three experiments produced significantly better results than a random classification. McNemar tests illustrate that the improvements from hyperspectral imagery and bathymetry data were significant. Comparison between group-level and code-level results shows a decreasing accuracy with increasing habitat complexity.

4.2. Results from different classifiers and ensemble analysis

From the above experimental analysis, we can see that a combination of hyperspectral imagery, aerial photograph, and bathymetry data achieved the best result. Thus the SVM and k-NN algorithms were only applied to the fused dataset of three data sources. For the SVM algorithms, after a number of trials using polynomial and RBF kernels, the polynomial kernel with the degree parameter (p) set to 2 and penalty error parameter (C) set to 2.0 generated the best result. For the k-NN method, k was specified to 3 after several trails. The final results from these two classifiers are also listed in Table 1 as Experiments 4 and 5 for SVM and k-NN respectively. SVM produced a relatively lower accuracy and k-NN generated the same overall accuracy as the RF classifier for both level classifications. Kappa statistical tests show that SVM and k-NN were significantly better than a random classification. McNemar tests reveal that RF was significantly better than SVM. There was no significant difference in accuracy between RF and k-NN.

The per-class accuracy from RF, SVM, and k-NN are shown in Tables 2 and 3. For the group-level classification (Table 2), SVM produced the same accuracy as the RF classifier in identifying hard-bottom and continuous seagrass, but yielded a lower accuracy in

Table 1
Classification accuracies and statistical tests using different datasets and classifiers.

Experiment #	Overall accuracy (%)	Kappa value	z-Score (Kappa)	z-Score (McNemar)
Group-level classification				
1	63.6	0.42	11.3	NA
2	86.3	0.78	29.2	8.30 (1/2)
3	88.5	0.82	32.8	1.88 (2/3)
4	82.2	0.72	24.3	3.43 (3/4)
5	88.5	0.82	32.8	0.00 (3/5)
6	89.6	0.84	34.6	1.07 (3/6)
Code-level classification				
1	57.0	0.44	14.3	NA
2	79.9	0.74	29.5	8.15 (1/2)
3	83.5	0.79	33.6	2.65 (2/3)
4	79.4	0.74	29.6	2.00 (3/4)
5	83.5	0.79	33.5	0.00 (3/5)
6	85.0	0.81	35.9	1.22 (3/6)

Notes:
Experiment 1 used DOQQ alone and RF classifier.
Experiment 2 used fused hyperspectral and aerial photograph data and RF classifier.
Experiment 3 used fused hyperspectral, aerial photograph, and bathymetry data and RF classifier.
Experiment 4 used fused hyperspectral, aerial photograph, and bathymetry data and SVM classifier.
Experiment 5 used fused hyperspectral, aerial photograph, and bathymetry data and k-NN classifier.
Experiment 6 used fused hyperspectral, aerial photograph, and bathymetry data and ensemble analysis of three classifiers.
The critical value of z-score is 1.96 at a confidence level of 0.95.

Table 2
Group-level per-class accuracy from different classifiers.

Group	Accuracy (%)		
	RF	SVM	*k*-NN
Hardbottom	95.6	95.6	95.4
Continuous seagrass	77.6	77.6	80.4
Patchy seagrass	87.6	63.8	86.7

Table 3
Code-level per-class accuracy from different classifiers.

Code	Accuracy (%)		
	RF	SVM	*k*-NN
HC	88.9	94.4	88.9
HS	92.0	86.2	92.0
HSb	76.0	60.0	56.0
SD	89.9	86.1	87.3
SDb	50.0	57.7	61.5
SDB	25.0	62.5	62.5
SDBb	92.9	89.3	92.9
SPH	67.5	55.0	70.0
SS	33.3	33.3	33.3

discriminating patchy seagrass. RF produced a higher accuracy than *k*-NN in discriminating hardbottom and patchy seagrass, but generated a lower accuracy in classifying continuous seagrass. Similarly, the accuracies were different among three classifiers for the code-level classification (Table 3). SVM produced a higher accuracy than RF in classifying HC and SDB. *k*-NN yielded a higher accuracy than RF in identifying SDb and SPH. This suggests that combining three methods may improve the classification for their complementary strength in classifying different habitats. In fact, the difference in outputs from multiple classifiers is an assumption of classifier ensemble techniques. The ensemble analysis result is shown as Experiment 6 in Table 1. It indeed increased the accuracy for both level classifications, although the improvements were marginal. For the group-level classification, the overall accuracy was increased from 88.5% to 89.6% with a Kappa value of 0.84, while for the code-level classification the overall accuracy was increased from 83.5% to 85.0% with a Kappa value of 0.81. But McNemar tests show that these improvements were not significant with a *z*-score of 1.07 and 1.22 for group-level and code-level classification respectively.

4.3. Object-based habitat mapping

According to Fleiss (1981) Kappa values larger than 0.75 suggest strong agreement. Landis and Koch (1977) suggest that Kappa values larger than 0.81 indicate an almost perfect agreement. The designed framework produced the Kappa values of 0.84 and 0.81 for the group-level and code-level classifications respectively, indicating it is effective for benthic habitat mapping in the Florida Keys. Object-based habitat maps were thus produced using the final fused dataset and ensemble analysis of RF, SVM, and *k*-NN, as shown in Fig. 3b (bottom panels). The object-based habitat maps are more informative and useful than a traditional pixel-based one that may be noisy if the study area has a high degree of spatial and spectral heterogeneity. For comparison, the reference maps are shown as Fig. 3a (top panels). There is a general agreement on the spatial distribution of habitat types between the reference and classified maps, with many regions accurately denoted. Further examination reveals some areas were misclassified, such as the southeast corner in the code-level maps (right panels). It is difficult to determine which map is better given the fact that the reference map was generated by manual interpretation and compilation of aerial photos. Errors and uncertainties are also unavoidable in the interpretation procedure. The error matrixes for the classified maps are displayed in Tables 4 and 5. For the group-level classification, the producer's accuracies (PA) changed from 80.4% to 97.8% and the user's accuracies (UA) varied from 88.5% to 91.6% (Table 4). For the code-level classification, the PA varied from 33.3% to 94.4% and the UA changed from 58.8% to 100% (Table 5).

Table 4
Error matrix for the group-level classification.

Group #	1	2	3	Row total	PA (%)
1	177	3	1	181	97.8
2	14	86	7	107	80.4
3	9	7	89	105	84.8
Col. Total	200	96	97	Overall accuracy: 89.6%	
UA (%)	88.5	89.6	91.6	Kappa value: 0.84	

UA: User's Accuracy; PA: Producer's Accuracy.
Classification result is displayed in row, and the reference data is displayed in column.
Groups 1–3 represent for hardbottom, continuous seagrass, and patchy seagrass respectively.

5. Discussion and summary

5.1. Benefits of data fusion in benthic habitat mapping

Most benthic habitat mapping studies examine single data source or compared the applicability of multiple data sources. Examples include the application of fine spatial resolution satellite imagery collected from IKONOS or QuickBird (e.g., Mumby and Edwards, 2002; Andréfouët et al., 2003; Mishra et al., 2006; Phinn et al., 2012; Zapata-Ramírez et al., 2013). Few attempts have been made to combine multiple data sources in the mapping efforts. Using very high spatial resolution aerial imagery (4 m or smaller) alone could not produce adequate accuracy for a fine descriptive detail (Benfield et al., 2007). This is also confirmed by this study. High spectral resolution hyperspectral imagery is useful in discriminating habitat communities at a finer detail, but its moderate spatial resolution may limit its broader application. To mitigate this problem, a combination of two data sources was examined. Hyperspectral imaging relies primarily on spectral features to discriminate covers, whereas very fine spatial resolution imagery relies more on spatially invariant features to identify targets (Shaw and Burke, 2003). A combination of two sources should have better performance in habitat mapping. The study illustrates that the integration of very high spatial resolution aerial imagery and hyperspectral data has a good performance in habitat classification. Water depth is believed to be an important factor that influences benthic covers in a reef environment (Bertels et al., 2008) and has been frequently included in the manual mapping procedure (e.g., Rohmann and Monaco, 2005). This drives the inclusion of bathymetry data in the framework. The study indicates that the contribution of bathymetry data is statistically significant for the code-level classification, but not significant for the group-level classification. The fused dataset from three data sources has been proved more powerful for habitat classification. The designed data fusion scheme is able to complement the shortages and take advantage of the benefits of each individual data source. The developed pixel/feature-level fusion strategy successfully combines the spatial features of aerial photograph, spectral contents of hyperspectral imagery, and elevation information of bathymetry data at the object level. Small patches and habitat types with linear/narrow shapes could be better discerned with the fused data.

Table 5
Error matrix for the code-level classification.

Code	HC	HS	HSb	SD	SDb	SDB	SDBb	SPH	SS	Row Total	PA (%)
HC	17	1								18	94.4
HS	1	127	7		2		1			138	92.0
HSb	1	3	20					1		25	80.0
SD		5		71			2	1		79	89.9
SDb		2	5	3	15		1			26	57.7
SDB				3		3	2			8	37.5
SDBb				2	1		53			56	94.6
SPH		7	2	3	1			27		40	67.5
SS	1						1		1	3	33.3
Col. Total	20	145	34	82	19	3	60	29	1	Overall accuracy: 85.0%	
UA (%)	85.0	87.6	58.8	86.6	79.0	100.0	88.3	93.1	100.0	Kappa value: 0.81	

UA: User's Accuracy; PA: Producer's Accuracy.
Classification result is displayed in row, and the reference data is displayed in column.

5.2. Advantages of machine learning classifiers and ensemble analysis

Previous benthic habitat mapping research focuses on the application of Maximum Likelihood method which could not produce high accuracy, especially in classifying the fused dataset from multiple data sources. A recent study from Zhang et al. (2013) illustrates that RF is able to produce higher classification accuracy than Maximum Likelihood in benthic habitat mapping using hyperspectral imagery. The RF classifier was adopted for this study to further examine its performance. Another two machine learning algorithms, SVM and k-NN, was also explored here. All three classifiers had a good performance. The RF and *k*-NN achieved the same classification accuracy and the SVM present a comparable result with RF and *k*-NN. Three classifiers showed a diversity in per-class accuracy, which is primarily caused by the discrepancies in concepts of three methods. RF looks for optimal decision trees to group data, whereas SVMs look for the optimal hyperplane to categorize data and *k*-NN searches for the best match to denote inputs. Note that the classification diversity is the basic assumption of ensemble systems, which drives me to explore the potential of an ensemble analysis. Indeed the ensemble approach achieved higher classification accuracy than three classifiers used. The improvement, however, was marginal and insignificant. Although the difference in accuracy was not statistically significant, the ensemble approach can provide some complementary information to the error matrix of the classified maps (Zhang, 2014). An index of classification uncertainty can be derived based on the votes of the classifiers. For example, if three votes are same for an input image object, a value of 3 will be assigned to this object. Conversely a value of 2 or 1 will be assigned to an input image object when two votes are same or three votes are completely different. This type of uncertainty maps is useful when there is a desire to minimize the omission or commission errors. It also can be used to guide the post-classification fieldwork (Foody et al., 2007).

5.3. Summary

In summary, a framework was designed to combine three data sources (hyperspectral, aerial photography, and bathymetry data) and four data processing techniques (data fusion, Object-based Image Analysis, machine learning, and ensemble analysis) for benthic habitat mapping in a coral reef ecosystem. A pixel/feature-level fusion strategy was developed to integrate three data sources. The framework was applied to map the benthic habitats in the Florida Keys. An overall accuracy of 89.6% and 85.0% was achieved at the group-level (3 classes) and code-level (9 classes) classifications. The designed framework has potential to map habitats over larger areas, because the spaceborne hyperspectral sensors (e.g., EO-1/Hyperion) and very fine spatial resolution multispectral sensors (e.g., QuickBird and IKONOS) have similar spatial and spectral characteristics as the data used in this study (i.e. AVIRIS and aerial photography). Bathymetry data is also available for the Florida Keys as well as many other coral reef areas. The in-orbit EO-1/Hyperion is providing 30-m hyperspectral imagery with 220 bands to the public at no cost. NAPP collects fine spatial resolution aerial photos at the national level with an approximate time frequency of five years, and also provides free high quality DOQQ data to the public. Local government agencies frequently collect large-scale aerial photography in the Florida Keys for coral reef protection and conservation. The framework is assumed to be useful for monitoring coral reefs, building or updating benthic habitat maps at reduced expenses using multiple data sources.

The framework can be also applied for the land cover classification with minor modifications to combine very high spatial resolution aerial photography, high spatial resolution (20–30 m) hyperspectral imagery and other data sources such as LiDAR, DEM, and geo-environmental data. A recent study from Zhang and Xie (2013a) finds that fusing hyperspectral imagery with DOQQ data can increase mapping accuracy of vegetation in a heterogeneous wetland environment. For benthic habitat mapping, inclusion of water quality parameters in the framework may further improve the classification accuracy. Similarly, combining more advanced classifiers such as neural networks may be helpful as well. In addition, considerable additional work is needed to investigate whether the developed framework can be used in other shallow waters. These will be major dedications in the future work. It is anticipated that this study can benefit the global coral reef monitoring and mapping in general, and the Florida Keys in particular.

Appendix A

Descriptions of the habitats found in the selected study area (from Benthic Habitats of the Florida Keys, <http://flkeysbenthicmaps.noaa.gov/>).

Groups	Codes
Hardbottom	*HC: Soft coral, hard coral, sponge, algae* Benthic community (no perceptible seagrass) is variable and typically a function of sediment, water, depth, and exposure to wind and current. It may also include solitary hard

(*continued on next page*)

Appendix A (*continued*)

Groups	Codes
	corals, *Porites* sp., *Sideratrea* sp., and *Manicina* sp. Shallowest zones (<1 m) may include only attached or drift algae; soft corals are usually more common in deeper zones *HS: Hardbottom with perceptible seagrass (<50%)* Usually in patches, seagrasses occur in depressions and basins where adequate sediment has accumulated, but constitute <50% bottom coverage. Hardbottom may include solitary hard corals and soft corals, but most often sponges and benthic algae (attached or in draft)
Continuous Seagrass	*SD: Moderate to dense, continuous beds* Solid, continuous *Thalassia*, *Syringodium*, and *Halodule*, individually or in mixed beds. Widespread in occurrence with range in depth from intertidal (bank) to approximately 10 m *SDB: Moderate to dense, nearly continuous beds (seagrass >50%), with blowouts and/or sand or mud patches* Solid, continuous *Thalassia* or *Syringodium*, rarely *Halodule*, individually or in mixed beds. Widespread in occurrence with range in depth from intertidal (bank) to approximately 10 m. Moderate to high energy regimes. Here, blowouts or patches are dispersed as holes in otherwise continuous seagrass beds. Usually found on reef tract and near entrances to tidal channels and passes. A common habitat in back country of middle keys with large water movements between the Gulf of Mexico and Atlantic Ocean *SS: Sparse, continuous beds* Areas where seagrasses occur in low density. Typically in shallow protected bays where physical conditions or substrate limits development. It may be hard to distinguish signature on aerial photographs from barren bottom, requiring ground truthing
Patchy Seagrass	*SPH: Dense patches of seagrass (>50%) in a matrix of hardbottom* One of the most common habitat types; patches occur in areas where a thin sediment layer over flat natural rock precludes development of seagrasses. Often numerous in number, highly visible on aerial photographs

Notes: A special modifier "b" is attached to a specific code type to indicate banks when applicable. For example HSb, SDb, and SDBb. Description: Intertidal seagrass and some hardbottom communities, even if only intertidal at spring low tides, often open water features or extending out from a shoreline. Distinctive signature on aerial photography is compared to surrounding bottom. Sometimes burned off patches are present on bank top. If these patches become large enough, they are mapped as separate bare areas.

References

Andréfouët, S., Kramer, P., Torres-Pulliza, D., Joyce, K.E., Hochberg, E.J., Garza-Perez, R., Mumby, P.J., Riegl, B., Yamano, H., White, W.H., Zubia, M., Brock, J.C., Phinn, S.R., Naseer, A., Hatcher, B.G., Muller-Karger, F.E., 2003. Multi-sites evaluation of IKONOS data for classification of tropical coral reef environments. Remote Sens. Environ. 88, 128–143.

Benfield, S.L., Guzman, H.M., Mair, J.M., Young, J.A.T., 2007. Mapping the distribution of coral reefs and associated sublittoral habitats in Pacific Panama: a comparison of optical satellite sensors and classification methodologies. Int. J. Remote Sens. 28, 5047–5070.

Benthic habitats of the Florida Keys, <http://flkeysbenthicmaps.noaa.gov/>, (accessed 17 04 13).

Benz, U., Hofmann, P., Willhauck, G., Lingenfelder, I., Heynen, M., 2004. Multiresolution, object-oriented fuzzy analysis of remote sensing data for GIS-ready information. ISPRS J. Photogrammetry Remote Sens. 58, 239–258.

Bertels, L., Vanderstraete, T., Coillie, S.V., Knaeps, E., Sterckx, S., Goossens, R., Deronde, B., 2008. Mapping of coral reefs using hyperspectral CASI data; a case study: Fordata, Tanimbar, Indonesia. Int. J. Remote Sens. 29, 2359–2391.

Blaschke, T., 2010. Object based image analysis for remote sensing. ISPRS J. Photogrammetry Remote Sens. 65, 2–16.

Botha, E.J., Brando, V.E., Anstee, J.M., Dekker, A.G., Sagar, S., 2013. Increased spectral resolution enhances coral detection under varying water conditions. Remote Sens. Environ. 131, 247–261.

Breiman, L., 2001. Random forests. Machine Learning 45, 5–32.

Chan, J.C.-W., Paelinckx, D., 2008. Evaluation of random forest and Adaboost tree based ensemble classification and spectral band selection for ecotope mapping using airborne hyperspectral imagery. Remote Sens. Environ. 112, 2999–3011.

Chang, C-C., Lin, C.-J., 2011. LIBSVM: A library for support vector machines. ACM Transactions on Intelligent Systems and Technology, <http://www.csie.ntu.edu.tw/~cjlin/libsvm>, (accessed 14 06 13).

Congalton, R., Green, K., 2009. Assessing the Accuracy of Remotely Sensed Data: Principles and Practices, second Edition. CRC/Taylor & Francis, Boca Raton, Florida.

Du, P., Xia, J., Zhang, W., Tan, K., Liu, Y., Liu, S., 2012. Multiple classifier system for remote sensing image classification: a review. Sensors 12, 4764–4792.

Fearns, P.R.C., Klonowski, W., Babcock, R.C., England, P., Phillips, J., 2011. Shallow water substrate mapping using hyperspectral remote sensing. Cont. Shelf Res. 31, 1249–1259.

Fleiss, J.L., 1981. Statistical Methods for Rates and Proportions, second Ed. John Wiley & Sons, New York.

Florida Keys National Marine Sanctuary (FKNMS), <http://floridakeys.noaa.gov/>, (accessed on 17. 04. 13).

Foody, G.M., 2004. Thematic map comparison, evaluating the statistical significance of differences in classification accuracy. Photogrammetric Eng. Remote Sens. 70, 627–633.

Foody, G.M., Boyd, D.S., Sanchez-Hernandez, C., 2007. Mapping a specific class with an ensemble of classifiers. Int. J. Remote Sens. 28, 1733–1746.

Green, A.A., Berman, M., Switzer, P., Craig, M.D., 1988. A transformation for ordering multispectral data in terms of image quality with implications for noise removal. IEEE Trans. Geosci. Remote Sens. 26, 65–74.

Grothe, P.R., Taylor, L.A., Eakins, B.W., Carignan, K.S., Friday, D.Z., Lim, E., Love, M.R., 2011. Digital Elevation Models of Key West, Florida: Procedures. Data Sources and Analysis, NOAA National Geophysical Data Center Technical Report, Boulder, CO, 20 pp.

Ham, J., Chen, Y., Crawford, M.M., Ghosh, J., 2005. Investigation of the random forest framework for classification of hyperspectral data. IEEE Trans. Geosci. Remote Sens. 43, 492–501.

Hardin, P.J., 1994. Parametric and nearest-neighbor methods for hybrid classification: a comparison of pixel assignment accuracy. Photogrammetric Eng. Remote Sens. 60, 1439–1448.

Hsu, C., Chang, C., Lin, C., 2010. A practical guide to support vector classification. Final report. National Taiwan University, Taipei City, Taiwan.

Huang, C., Davis, L.S., Townshend, J.R.G., 2002. An assessment of support vector machines for land cover classification. Int. J. Remote Sens. 23, 725–749.

Johnson, B., Xie, Z., 2011. Unsupervised image segmentation evaluation and refinement using a multi-scale approach. ISPRS J. Photogrammetry Remote Sens. 66, 473–483.

Landis, J., Koch, G.G., 1977. The measurement of observer agreement for categorical data. Biometics 33, 159–174.

Lesser, M.P., Mobley, C.D., 2007. Bathymetry, water optical properties, and benthic classification of coral reefs using hyperspectral remote sensing imagery. Coral Reefs 26, 819-819.

Mishra, D., Narumalani, S., Rundquist, D., Lawson, M., 2006. Benthic habitat mapping in tropical marine environments using QuickBird multispectral data. Photogrammetric Eng. Remote Sens. 72, 1037–1048.

Mishra, D., Narumalani, S., Rundquist, D., Lawson, M., Perk, R., 2007. Enhancing the detection and classification of coral reef and associated benthic habitats: a hyperspectral remote sensing approach. J. Geophys. Res. 112, C08014. http://dx.doi.org/10.1029/2006JC003892.

Moreno-Seco, F., Iñesta, J., de León, P., Micó, L., 2006. Comparison of classifier fusion methods for classification in pattern recognition tasks. In: Proceedings of the 2006 joint IAPR international conference on Structural, Syntactic, and Statistical Pattern Recognition, pp. 705–713.

Mountrakis, G., Im, J., Ogole, C., 2010. Support vector machines in remote sensing: a review. ISPRS J. Photogrammetry Remote Sens. 66, 247–259.

Mumby, P.J., Edwards, A.J., 2002. Mapping marine environments with IKONOS imagery: enhanced spatial resolution does deliver greater thematic accuracy. Remote Sens. Environ. 82, 248–257.

Phinn, S., Roelfsema, C., Dekker, A., Brando, V., Anstee, J., 2008. Mapping seagrass species, cover and biomass in shallow waters: an assessment of satellite multispectral and airborne hyper-spectral imaging systems in Moreton Bay (Australia). Remote Sens. Environ. 112, 3413–3425.

Phinn, S.R., Roelfsema, C.M., Mumby, P.J., 2012. Multi-scale, object-based image analysis for mapping geomorphic and ecological zones on coral reefs. Int. J. Remote Sens. 33, 3768–3797.

Pu, R., Bell, S., Meyer, C., Baggett, L., Zhao, Y., 2012. Mapping and assessing seagrass along the western coast of Florida using Landsat TM and EO-1 ALI/Hyperion imagery. Estuar. Coast. Shelf Sci. 115, 234–245.

Rohmann, S. O., Monaco, M. E., 2005. Mapping Southern Florida's Shallow-water Coral Ecosystems: An Implementation Plan. NOAA Technical Memorandum NOS NCCOS 19. NOAA/NOS/NCCOS/CCMA. Silver Spring, MD.

Shaw, G.A., Burke, H.K., 2003. Spectral imaging for remote sensing. Lincoln Lab. J. 14, 3–28.

Solberg, A.H.S., 2006. Data fusion for remote sensing applications. In: Chen, C.H. (Ed.), Signal and Image Processing for Remote Sensing. CRC Press, Boca Raton, FL, pp. 515–537.

Trimble, 2011. eCognition Developer 8.64.1 reference book.

Vapnik, V.N., 1995. The Nature of Statistical Learning Theory. Springer-Verlag, New York.

Warner, T., 2011. Kernel-based texture in remote sensing image classification. Geography Compass 5, 781–798.

Waske, B., Benediktsson, J.A., Árnason, K., Sveinsson, J.R., 2009. Mapping of hyperspectral AVIRIS data using machine-learning algorithms. Can. J. Remote Sens. 35, S106–S116.

Waske, B., Fauvel, M., Benediktsson, J. A., Chanussot, J., 2009. Machine learning techniques in remote sensing data analysis. In: G. Camps-Valls and L. Bruzzone (Eds.), Kernel Methods for Remote Sensing Data Analysis, John Wiley & Sons Ltd, Chichester, UK. doi:10.1002/9780470748992.ch1.

Zapata-Ramírez, P.A., Blanchon, P., Olioso, A., Hernandez-Nuñez, H., Sobrino, J.A., 2013. Accuracy of IKONOS for mapping benthic coral-reef habitats: a case study from the Puerto Morelos Reef National Park, Mexico. Int. J. Remote Sens. 34, 3671–3687.

Zhang, J., 2010. Multi-source remote sensing data fusion: status and trends. Int. J. Image Data Fusion 1, 5–24.

Zhang, C., 2014. Combining hyperspectral and LiDAR data for vegetation mapping in the Florida Everglades. Photogrammetric Engineering & Remote Sensing 80, 21–31.

Zhang, C., Xie, Z., 2012. Combining object-based texture measures with a neural network for vegetation mapping in the Everglades from hyperspectral imagery. Remote Sens. Environ. 124, 310–320.

Zhang, C., Xie, Z., 2013a. Data fusion and classifier ensemble techniques for vegetation mapping in the coastal Everglades. Geocarto Int. http://dx.doi.org/10.1080/10106049.2012.756940.

Zhang, C., Xie, Z., 2013b. Object-based vegetation mapping in the Kissimmee River watershed using HyMap data and machine learning techniques. Wetlands 33, 233–244.

Zhang, C., Selch, D., Xie, Z., Roberts, C., Cooper, H., Chen, G., 2013. Object-based benthic habitat mapping in the Florida Keys from hyperspectral imagery. Estuar. Coast. Shelf Sci. 134, 88–97.